NANO · MICRO small
www.small-journal.com

Printing of In Situ Functionalized Mesoporous Silica with Digital Light Processing for Combinatorial Sensing

*Lucy Zhao, Dieter Spiehl, Marion C. Kohnen, Marcelo Ceolin, Joanna J. Mikolei, Raheleh Pardehkhorram, and Annette Andrieu-Brunsen**

Combinatorial sensing is especially important in the context of modern drug development to enable fast screening of large data sets. Mesoporous silica materials offer high surface area and a wide range of functionalization possibilities. By adding structural control, the combination of structural and functional control along all length scales opens a new pathway that permits larger amounts of analytes being tested simultaneously for complex sensing tasks. This study presents a fast and simple way to produce mesoporous silica in various shapes and sizes between 0.27–6 mm by using light-induced sol-gel chemistry and digital light processing (DLP). Shape-selective functionalization of mesoporous silica is successfully carried out either after printing using organosilanes or in situ while printing through the use of functional mesopore template for the in situ functionalization approach. Shape-selective adsorption of dyes is shown as a demonstrator toward shape selective screening of potential analytes.

1. Introduction

Combinatorial chemistry is used for accelerating modern drug development[1] or in discovering and optimizing new materials.[2] For this purpose, fast screening and decoding of combinatorial libraries are essential. Further improvement of efficiency can be achieved by combinatorial sensing. For example, screen-printed carbon electrodes can simultaneously detect different species by using their electrochemical characteristics.[3] Miniaturizing of sensors allows high-throughput screening systems. For example, nanodroplets allow parallelized on-chip solution-based synthesis or biological screening.[4] Using microarrays has proven to be an effective screening system for identifying novel antibacterial compounds.[5] Among other materials, modified porous support materials are suitable for high-throughput applications due to their high specific surface area allowing high loading densities of active components.[6] Mesoporous inorganic and organic–inorganic hybrid films have attracted growing interest due to their versatile potential in biotechnological applications,[7] electrochemical energy storage and conversion,[8] catalysis[9] as well as sensing.[10] Fabrication of mesoporous silica films is in most cases based on Evaporation-Induced Self-Assembly (EISA).[11,12] Nevertheless, its complex processing, the relatively high amount of solvents, and the required high temperature post-treatment are disadvantages.[13] Croutxé-Barghorn, Chemtob, and colleagues have presented a simple alternative approach to obtain mesoporous silica films, in which mesostructured formation is independent of solvent evaporation, but UV light is used instead to trigger micelle formation of amphiphilic block copolymers. Up to 3–4 µm thick mesostructured organic–inorganic hybrid silica films were prepared by using this so-called Light-Induced Self-Assembly (LISA) upon UV light irradiation.[14] Different solution compositions (block copolymer template, poly(dimethoxysiloxane) (PDMOS), photoacid generator (PAG)) and other parameters, such as surrounding humidity or irradiation[15] were systematically studied with respect to the mesostructured formation. Scaling-up of the UV light induced self-assembly process for obtaining micrometer-thick mesoporous silica films (>100 cm^2) was achieved under specific conditions regarding the obtained film thickness, the applied humidity, and templating agent concentration.[16] Although thick hybrid mesostructured silica films were obtained, decreasing the film thickness below 1 µm allowed the forming of crack-free films after thermal surfactant removal.[16] An alternative method to calcinate the mesopore template is to use UV light instead of temperature.[17] To further develop this process toward

L. Zhao, D. Spiehl, M. C. Kohnen, J. J. Mikolei, R. Pardehkhorram, A. Andrieu-Brunsen
Ernst-Berl Institut für Technische und Makromolekulare Chemie
Makromolekulare Chemie – Smart Membranes
Peter-Grünberg-Str. 8, D-64287 Darmstadt, Germany
E-mail: annette.andrieu-brunsen@tu-darmstadt.de
D. Spiehl
Institut für Druckmaschinen und Druckverfahren – IDD
Technische Universität Darmstadt
Magdalenenstr. 2, D-64289 Darmstadt, Germany
M. Ceolin
Instituto de Investigaciones Fisicoquímicas Teóricas y Aplicadas
Universidad Nacional de La Plata and CONICET
Diag. 113 y 64, La Plata B1900, Argentina

The ORCID identification number(s) for the author(s) of this article can be found under https://doi.org/10.1002/smll.202311121

DOI: 10.1002/smll.202311121

being more environmentally friendly, LEDs have become increasingly recognized for inducing less undesired heating while being more energy efficient. By using photosensitizers the absorption wavelength of the PAG can be shifted to match the spectrum of visible LEDs which was first used to activate the sol-gel process for the synthesis of inorganic films in 2015.[18] The synthesized inorganic films as coatings were limited in their size by the film applicator and light source, while no shaping on macroscopic level was achieved.

In addition to demonstrating light-induced silica formation, shaping different silica objects has been shown by the use of the additive manufacturing methods stereolithography (SLA),[19] digital light processing (DLP),[20–22] and two-photon polymerization (TPP).[23] Transparent fused silica glass was obtained in a 3D printing process by Kotz et al. using a mixture of silica nanoparticles and photocurable monomers for a free radical polymerization.[19] Two examples using a so-called hybrid ceramic precursor in combination with other conventional sol-gel precursors, such as tetramethyl orthosilicate (TMOS) or trimethoxymethylsilane (MTMS), are shown by Cooperstein et al. and Shukrun et al.[20,21] Hybrid precursor in this case refers to a component, which can undergo both a sol-gel process of metal-alkoxide groups as well as a photo polymerization process due to a second functional group such as 3-acryloxypropyl trimethoxysilane (APTMS). Using such hybrid precursors a fast shape formation upon radical polymerization is achieved and the comparably slow hydrolysis and condensation occur mainly during the post-treatment process.[21] Another approach to achieve high control during 3D printing was presented by Moore et al., applying photopolymerization-induced phase separation of hybrid resins.[22] In this specific example, hybrid resins composed of alkoxide inorganic precursors and photoactive monomer mixture being capable to undergo a radical polymerization upon irradiation were used. The as-printed hybrid shapes were pyrolyzed to form a nanoscale porous structure with strut dimensions of 320–150 nm that can further be sintered into transparent multi-material glasses.[22] Mesoporous silica shapes were first fabricated with 3D resolution by Shukrun et al. in 2020 upon mixing a silica precursor, a structure-directing agent, and an elastomer-forming ink with a photocurable monomer inducing a radical polymerization.[24] The photocurable radical polymerizable monomer enabled shaping of the hybrid material and entrapped the sol-gel solution within the radically polymerized polymer network. During 1 week of aging at controlled environmental conditions the condensation proceeded while the solvent evaporated. A silica network shrinkage of 12 ± 5 vol% was observed. Subsequent calcination was used to remove the shape stabilizing photopolymer and a 3D shaped macroporous silica containing ordered mesopores was obtained. The calcination step results in an isotropic shrinkage of 62 ± 1 vol%. Different 3D mesoporous silica objects up to 1.5 cm in size have been realized by this method.[24] The same research group presented the use of a different ink composition without the need of an additional photocurable organic monomer as scaffold upon irradiation and replaced it with a hybrid precursor with an acrylic moiety (APTMS). This approach needed a complex post-treatment for obtaining the hybrid mesoporous structure, which consisted of solvent exchanges and supercritical drying.[23] To the best of our knowledge, these are the only examples demonstrating various approaches to shape mesoporous silica into 2D or 3D adjustable objects.

Here, we demonstrate printing of varying mesoporous silica shapes combining light-induced sol-gel chemistry with DLP without any radical polymerization for shape stabilization. With this approach of DLP-based printing of varying mesoporous silica shapes the process velocity is significantly improved to hours instead of days.[24] The LISA solution composition was first optimized to obtain transparent, free-standing mesoporous silica films. Mesoporous silica printing of varying shapes was achieved by application of LISA solution compositions in a two-step process of thin film deposition and subsequent irradiation in a DLP-based 3D printer. Printing process parameters were adjusted to obtain various mesoporous shapes with specific surface areas of 127–155 $m^2\ g^{-1}$. Reduction of exposure time and increase of shape accuracy was achieved upon further optimization of the solution composition. In situ functionalization of such printed mesoporous silica shapes has been realized by changing the mesopore template Pluronic P123 to a stimuli-responsive block copolymer as a functional template.[25] Besides in situ polymer functionalization using functional mesopore templates, the printed mesoporous silica shapes were successfully shape-selectively functionalized to allow component identification by shape detection or by fluorescence imaging based on its functionality for sensing application. Taking advantage of both characteristic recognition methods, relatively large amounts of analytes can be tested simultaneously. With this we expect our approach of shaping in situ functionalized mesoporous silica to accelerate screening processes and opening a new tool for combinatorial sensing.

2. Results and Discussion

To achieve printing of various free-standing mesoporous silica shapes with adjustable functional groups for analyte binding, mesoporous silica was prepared by DLP in a commercially available 3D printer. Therefore, the LISA process[16,18] was used (**Figure 1**).

As a first step the solution composition was optimized mainly to reduce the time needed for solidification. This parameter optimization was carried out on dip-coated thin films of the LISA solution deposited onto Si-wafer as a substrate followed by using a lamp (λ= 325–500 nm, 30 mW cm^{-2}) for irradiation and short resting time at ambient conditions before its application into the printer. The irradiation time and the following resting time were varied depending on the solution used. These reference experiments on dip-coated and subsequently irradiated films revealed a suitable solution composition of PDMOS as silica precursor, Pluronic P123 as mesopore template, diphenyliodonium hexafluorophosphate as PAG, isopropyl thioxanthone as photosensitizer (PS-I) and 30 wt% methanol : toluene solution (volume ratio 3:1) with respect to PDMOS. As the relative humidity is known to influence mesopore structure formation by determining the dissolved water content within the film which influences hydrolysis and condensation[16] the influence of water addition was investigated (**Figure 2**). The hydrolysis and condensation reaction of both solutions, with and without 1 vol% of added water, proceeded during and a short time after irradiation visible by solidification of the film. Depending on the exposure time

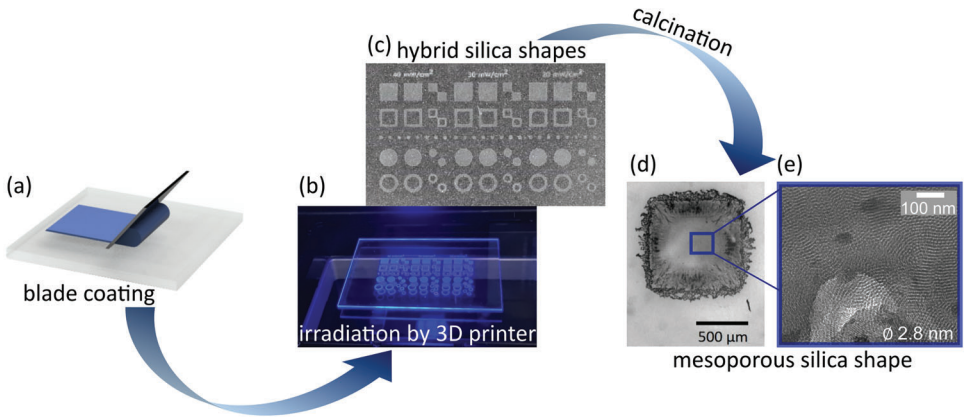

Figure 1. Schematic representation of the fabrication process of mesoporous silica shapes with DLP. The printing process starts with a) applying the LISA solution as a thin film on top of a glass substrate using blade coating. b) The DLP 3D printer projects a previously designed pattern onto the LISA thin film from beneath. c) The solidification of the LISA thin film takes place within the irradiated areas. The silica shapes containing template filled mesopores are detached from the glass substrate using a razor blade and subsequently undergo a thermal calcination to remove the mesopore template. This results in the mesoporous silica shape as indicated by d) the microscopy image and e) the TEM image.

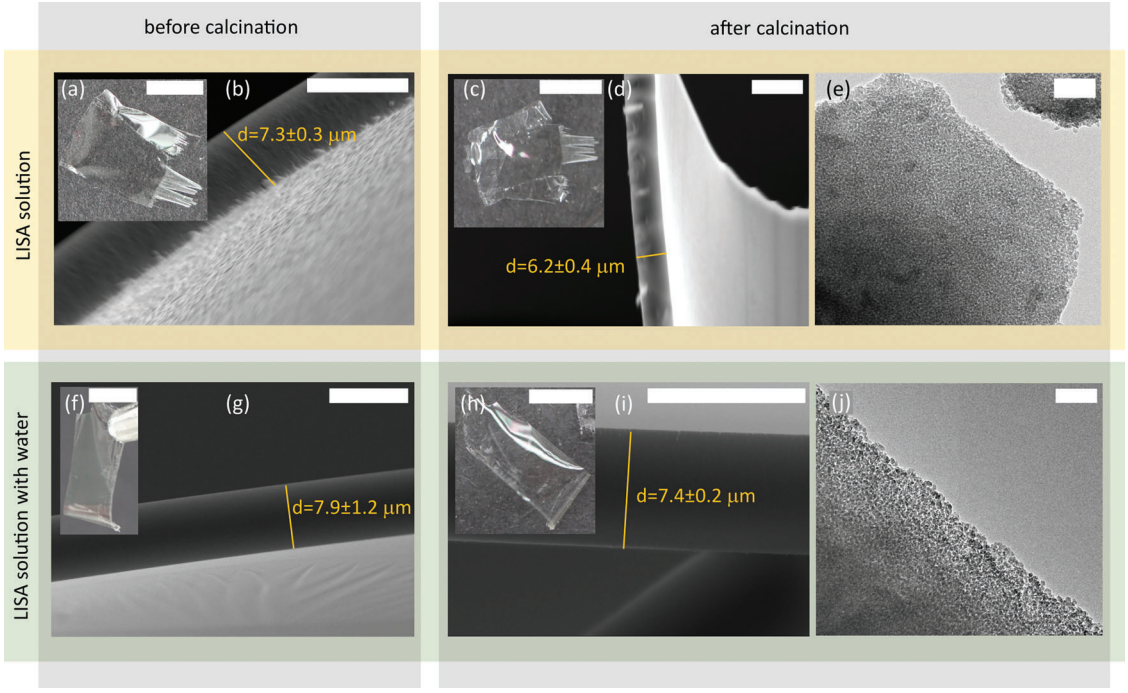

Figure 2. a) Image of free-standing silica film obtained from LISA solution (yellow) (scale bar 5 mm) and b) SEM image showing its cross-section and surface (scale bar 10 µm) before calcination. c) Image of free-standing silica film obtained from LISA solution after calcination at 250 °C for the removal of Pluronic P123 (scale bar 5 mm) and d) the corresponding SEM image (scale bar 10 µm). Both SEM images in comparison reveal the shrinkage in thickness of the free-standing silica film made from the LISA solution upon dip-coating and irradiation. The given thickness value results from averaging (b) 20 measurements of two samples and (d) 29 measurements of two samples. e) TEM image showing the presence of mesopores in the free-standing silica film after calcination (scale bar 100 nm). f) Image of free-standing silica film made from LISA solution by dip-coating and irradiation upon water addition (green) before calcination (scale bar 5 mm) and g) the corresponding SEM image (scale bar 10 µm). h) Image of free-standing silica film made from LISA solution by dip-coating and irradiation upon water addition (green) after calcination (scale bar 5 mm) and i) the corresponding SEM image (scale bar 10 µm). Thickness calculated from the mean of (g) 50 measurements of five samples and (i) 30 measurements of three samples. j) TEM showing the presence of mesopores in the free-standing silica film made from LISA solution by dip-coating and irradiation upon water addition after calcination (scale bar 100 nm).

the resting time at ambient temperature needed to be adjusted to achieve complete hydrolysis (Figure S1, Supporting Information). Interestingly, the solidified silica film can be detached from the substrate to obtain transparent, free-standing silica films with Pluronic P123 template filled mesopores, here referred to as a hybrid silica film. The irradiation time and the following resting time were varied depending on the used solution composition. The LISA solution without water was irradiated for 4 min and after 11 min resting time, the template filled mesoporous silica film was detached from the substrate (Figure 2a). When adding water to the LISA solution, the irradiation time was adjusted to 3 min and the resting time to 11 min (Figure 2f). The following calcination up to 250 °C resulted in successful removal of the mesopore template as deduced from the disappearing CH-vibrational bands ≈2900 cm^{-1} in the ATR-IR spectra (Figure S2, TGA of Pluronic P123 Figure S3, Supporting Information). The oven treatment at elevated temperature leads to further stabilization of the silica network due to condensation as deduced from the decreasing Si–OH vibrational band at 930 cm^{-1} in Figure S2 (Supporting Information) normalized ATR-IR spectra for mesoporous silica films as compared to the hybrid silica film before calcination.

Silica films synthesized with both solutions with and without water addition were analyzed by TGA which confirms an almost identical amount of the template Pluronic P123 as present in the LISA solution (Figure S4, Supporting Information). While transparency and observed macroscopic shape of the silica films are not affected by the calcination step (Figure 2c), it induces shrinkage and reduction in film thickness from 7.3 ± 0.2 to 6.2 ± 0.4 µm corresponding to a shrinkage of 15% of the original film thickness for mesoporous films prepared from the LISA solution without water addition (Figure 2b,d). Film thickness of mesoporous films prepared from the LISA solution with additional water decreases from 7.9 ± 1.2 to 7.4 ± 0.2 µm which corresponds to a shrinkage of 6% (Figure 2g,i). Besides film shrinkage along the film thickness no further defects were observed in SEM and TEM images (Figure 2). TEM images also confirm the obtained mesoporosity of the silica films (Figure 2e,j).

Therefore, both solutions were used to achieve printing of mesoporous silica shapes by DLP. For DLP-based mesoporous film printing the LISA solution was applied onto glass substrates using a doctor blade with a gap height of 20 µm. The created print pattern and mesoporous silica shapes includes filled or hollow squares and circles with varying sizes from 4.1 mm down to 1 mm edge length and diameter (**Figure** 3a), respectively. After exposure to light and resting time at ambient conditions the excess solution was removed by a washing step. The solidified shapes were removed from the glass substrate before the calcination step in order to allow shrinkage in all 3D. For this mesoporous silica printing procedure process parameters such as solution composition, substrate, light intensity and irradiation time, possible shapes, cleaning procedure, and calcination conditions were adjusted while depending on each other. For example, a water content of 1 vol% was identified as optimal with respect to solidification time and shape control of the printed mesoporous silica shapes (Figure S5, Supporting Information). The solution containing silica precursor was coated using a doctor blade onto a transparent glass substrate and the irradiation took place from the opposite side of the coated thin film. Although the applied glass substrates absorbed 5.1% of the irradiation power at 385 nm wavelength, the residual light intensity was sufficient for mesoporous silica printing. An illumination intensity of 30 to 40 mW cm^{-2} and an illumination time of 500 s was needed to solidify the applied precursor solution and to print mesoporous silica shapes. A resting time at ambient temperature of 5 min after illumination allowed further solidification. Followed by carefully rinsing with toluene to remove excess LISA solution and drying under clean compressed air resulted in mesoporous silica shapes with template filled pores in different shapes and dimensions. For example, filled or hollow circles and squares of 1 mm diameter and 4.1 mm edge length were produced as well as hollow shapes with a frame width of 270 to 675 µm (Figure 3). We used light microscopy to compare the dimensions of the printed silica shapes to the intended lateral size given by the number of pixels illuminated and the resolution of 27 µm $pixel^{-1}$ of the printer. This revealed silica shapes to be 5% ± 1% smaller than the illuminated areas which is ascribed to a slight dewetting of the solution on the glass substrate and shrinkage during the illumination-induced hydrolysis and condensation. The quality of the printed mesoporous silica shapes was not affected by this shrinkage. In addition, calcination for mesopore template removal induces a shrinkage of 15% ± 1% in the lateral dimensions of the samples (Figure 3c,d) as determined from several printed filled shapes. In *z*-direction, and thus along the shape thickness, a mean shrinkage in thickness of 34% from mean values of 3.2 ± 1.1 to 2.1 ± 0.8 µm upon calcination was determined from SEM cross-section images (Figure 3e,f). The printed mesoporous silica shapes show a relatively rough surface, and defect formation near the edge of the printed shapes (Figure 3e–i).

The printed silica shapes have a mesoporous structure, which is confirmed by the argon gas adsorption curve showing a type IV(a) isotherm with a hysteresis loop (Figure 3k).[26] According to argon gas adsorption measurement, the printed mesoporous silica shapes have a specific surface area of 127 m^2g^{-1}. The pore diameter is between 2.8 nm as determined by TEM (Figure 3i) and 4.7 nm with a pore size distribution of 2.5 nm as determined by argon gas adsorption measurement (Figure 3k,l). Mesopores are scattering centers that are arranged in a certain order with a regular distance of ≈15.7 nm, which is indicated by the broad Bragg peak at 0.04 A^{-1} in the SAXS measurement (Figure 3j). The regularity of the pore order is observed by TEM imaging, too (Figure 3i).

To further optimize the printed silica shapes by increasing the shape accuracy, reduction of irradiation time is needed as longer irradiation times favor acid diffusion and thus hydrolysis and condensation outside the intended areas. Irradiation time can be even further reduced to 25 s with constant irradiation intensity allowing smoother edges by increased amount of PAG and PS-I. Results obtained when printing from such a further optimized solution composition are shown in **Figure** 4.

Using the same pattern of filled or hollow circles and squares mesoporous silica shapes with higher resolution were printed showing sharper edges (Figure 4b,c). Compared to the targeted lateral size hollow shapes show a relatively high deviation being 23% ± 5% smaller than desired by the print pattern. Filled shapes are only 10% ± 3% smaller than intended. The subsequent calcination process for template removal induces a shrinkage with

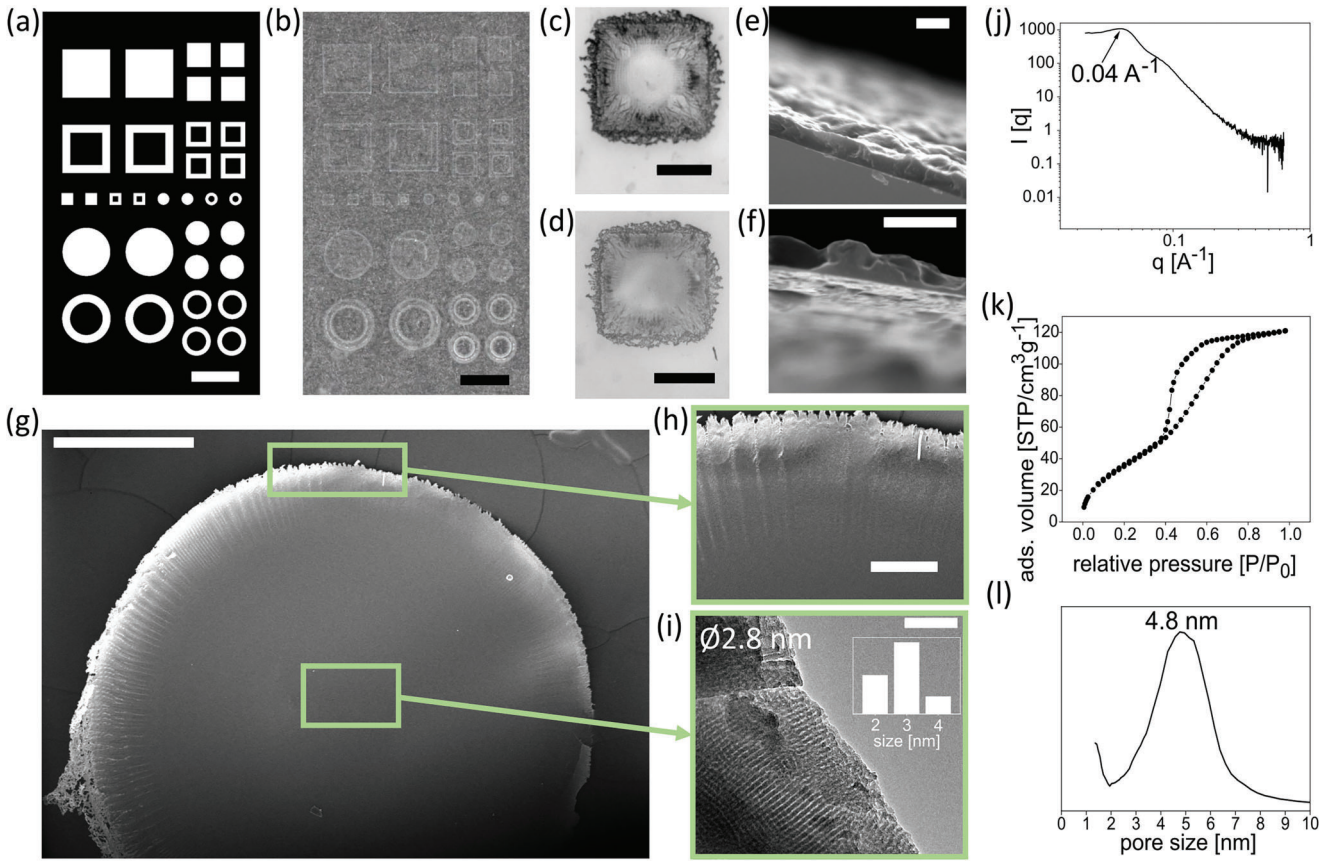

Figure 3. Overview on printed silica shapes made from the LISA solution with 1 vol% water: a) pattern of illumination by DLP (scale bar 4 mm), b) photograph of a printed pattern on a glass substrate after rinsing and drying (scale bar 4 mm, sample was placed on black paper for sufficient contrast to the background), microscopy image of the exact same printed shape c) before and d) after calcination for mesopore template removal at 250 °C (scale bars 500 µm). e,f) Cross-sectional SEM images of printed mesoporous silica shapes (e) before (averaging 22 measurements of five samples) and (f) after calcination (averaging 12 measurements of five samples) (scale bars 5 µm), g) SEM image (scale bar 1 mm) and h) magnified view (scale bar 200 µm) of a printed circular mesoporous silica shape after calcination. i) TEM image of the printed silica shape shows its porosity with an average pore diameter of 2.8 nm (scale bar 100 nm). j) SAXS measurement, k) argon gas sorption isotherm (127 m^2g^{-1}, R:0.9996), and l) determined pore size distribution of printed mesoporous silica shapes after calcination (most common pore size 4.8 nm, pore size distribution 2.5 nm, fitting error: 0.341%).

respect to the lateral dimensions of 15% ± 1% for filled shapes and 19% ± 6% for hollow silica shapes. Deviations are higher with hollow shapes due to their shape and stability. In *z*-direction, along the thickness, a mean shrinkage of 31% from 4.2 ± 0.5 to 2.9 ± 1.2 µm upon mesopore template calcination was observed. The shrinkage of filled shapes using both, optimized and non-optimized, LISA solution, lies within the same range (15% lateral, 34% *z*-direction, Figure 3). The absolute shape thickness is ≈1 µm thicker using the optimized LISA solution. This can be ascribed to the faster solidification and hence less residual solution being washed away after the resting time. The printed mesoporous shapes using the optimized LISA solution consist of wormlike mesopores as observed for mesoporous silica films prepared by using cetyltrimethylammonium bromide as structure-directing agent in the EISA process.[12] The pore diameter was determined by TEM to be 2.7 nm (Figure 4f), while argon gas adsorption measurement suggests pores with an average pore size of 4.8 nm and a pore size distribution of 1.9 nm (Figure 4i). The significantly reduced exposure time of 25 s influenced the mesopore formation as observed by TEM resulting in a less ordered mesopore arrangement. Although TEM may indicate less ordered mesopore arrangement, SAXS results still indicate ordered structure with shorter regular distances between the mesopores of ≈12.6 nm (Bragg peak at 0.05 A^{-1}, Figure 4g) as compared to the longer irradiation of the LISA solution (Figure 3j). Besides higher shape accuracy this optimized LISA solution shows narrower pore size distribution of 1.9 nm instead of 2.5 nm as determined by gas sorption measurements in case of longer irradiation time (Figure 3l), and a slightly larger specific surface area of 155 m^2 g^{-1} instead of 127 m^2 g^{-1} as compared to the printed shapes from the solution with lower amount of PAG and PS-I and longer irradiation time. Furthermore, this optimized LISA solution can be adapted to directly obtain in situ functionalized, mesoporous silica shapes from this printing approach. Here, poly(ethylene oxide)-*b*-poly(2-nitrobenzyl acrylate) (PEO_{42}-*b*-$PNBA_{13}$) was used replacing Pluronic P123 as mesopore template (**Figure 5**). PEO_{42}-*b*-$PNBA_{13}$ is of interest as it is cleavable upon light irradiation (λ= 254 nm) which allows time-dependent control of free carboxylic acid groups inside these highly filled mesopores (Figure S6, Supporting Information).[25]

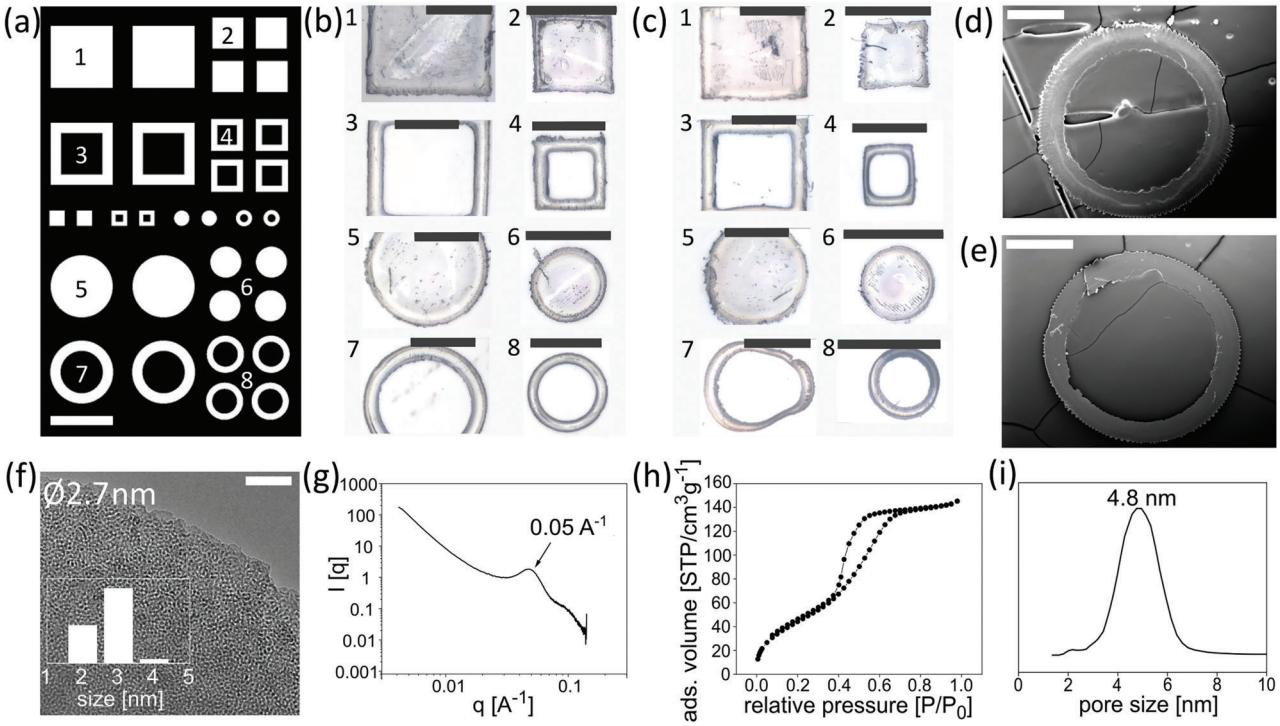

Figure 4. Overview on printed silica shapes by using the optimized LISA solution with an increased amount of PAG, PS-I, and 1 vol% water: a) pattern of illumination by DLP (scale bar 4 mm) (numbers integrated for illustration purpose and not during printing), b) microscopy images of different printed shapes before (scale bars 2 mm) and c) after the calcination step (scale bars 2 mm), SEM images of a hollow silica circle (shape #8) d) before and e) after calcination (scale bars 500 µm), f) TEM image of printed silica shape shows its porosity with an average pore diameter of 2.7 nm (scale bar 100 nm), g) SAXS measurement, h) argon gas sorption isotherm (155 m^2 g^{-1}, R:0.9997) and i) from this determined pore size distribution of printed mesoporous silica shape (most common pore size 4.8 nm, pore size distribution 1.9 nm, fitting error: 0.445%).

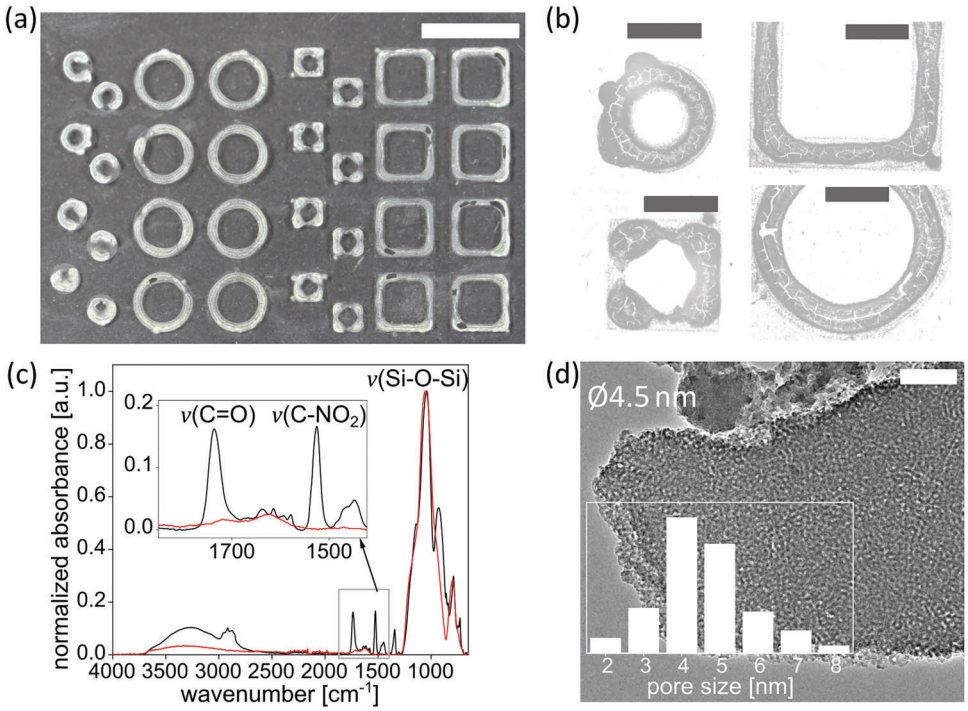

Figure 5. a) Image (scale bar 10 mm) and b) microscopy images (scale bars 2 mm) of different printed in situ PEO_{42}-*b*-$PNBA_{13}$ functionalized silica shapes. c) ATR-IR spectra of PEO_{42}-*b*-$PNBA_{13}$ functionalized silica shapes before (black) and after (red) PEO_{42}-*b*-$PNBA_{13}$ template removal upon calcination at 350 °C. d) TEM image ofmesoporous silica shape (scale bar 100 nm) after calcination for template removal.

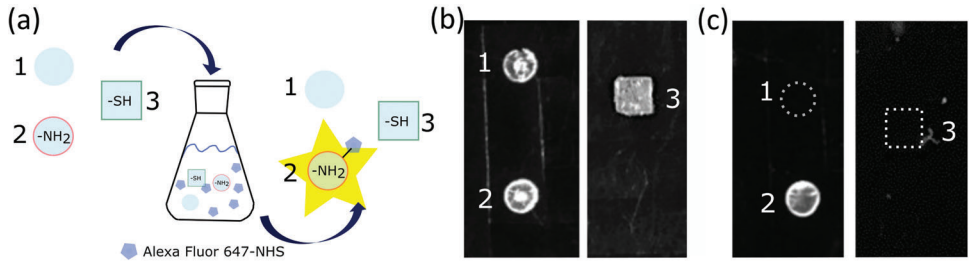

Figure 6. a) Schematic representation of the combinatory approach: 1) mesoporous silica circle, 2) amine-functionalized mesoporous silica circle, 3) thiol-functionalized mesoporous silica square. From these silica shapes only the amine-functionalized mesoporous silica circle should react with Alexa647-NHS. Fluorescence images of printed mesoporous silica shapes taken with b) no filters under white light as a reference, c) lighting and emission filters for Alexa647 (dotted lines indicate the position of the samples).

Various in situ PEO_{42}-*b*-$PNBA_{13}$ functionalized mesoporous silica shapes, hollow circles, and squares of 3–6 mm diameters and edge lengths, respectively, have been produced with a frame width of 0.9–2.1 mm (Figure 5a,b). The in situ PEO_{42}-*b*-$PNBA_{13}$ functionalization was successful as shown by the ATR-IR spectrum (Figure 5c, black). After PEO_{42}-*b*-$PNBA_{13}$ template calcination mesoporous silica was obtained (Figure 5c red, 5d). This mesoporous silica has an average pore size of 4.5 nm determined by TEM which is slightly smaller than the pore size of a mesoporous silica film obtained by using the same block copolymer via the EISA process (≈5.8 nm).[25] Here, we demonstrated in situ polymer functionalization of silica mesopores in combination with a shape-forming technique. The broad variety of functionalization methods of printed various mesoporous silica shapes is of interest, for example, in sensing for the combined analysis of shape and optical sensor response in combinatorial sensing. Printed mesoporous silica shapes of circular and square shape after calcination (prepared as shown in Figure 3) were functionalized by simple grafting-onto of (3-aminopropyl)triethoxysilane (APTES) or (3-mercaptopropyl)trimethoxysilane (MPTS), respectively. Specifically, the circular shaped mesoporous silica was functionalized with APTES while the mesoporous silica squares were functionalized with MPTS. Subsequently, amine-, thiol-, and non-functionalized silica shapes were incubated into Alexa Fluor 467-NHS dye solution which is expected to preferentially react with amine functionalized circular shaped mesoporous silica via click-chemistry. As demonstrated in **Figure 6**, after incubation of all three mesoporous silica shapes in the dye solution, a fluorescence signal is exclusively detected for these amine-functionalized mesoporous silica circles after illumination at λ= 640 nm (Figure 6c). Neither the unfunctionalized mesoporous silica circle or the thiol-functionalized silica square exhibit a fluorescence signal after incubation into the Alexa Fluor 647-NHS dye solution. This shows the potential of mesoporous silica printing of varying mesoporous silica shapes with shape specific functionalization for complex sensing and screening tasks. In case of ten differently shaped and specifically functionalized objects would react with 20 different analytes, 200 shape-analyte combinations would be identified in one step. Including complexity by, e.g., using possible multiple combinations into different shapes or mixed color generation even more analytes could be accessible. Together with machine learning-based techniques such an approach is expected to open new routes in analyte screening.

3. Conclusion

We presented the first example of silica printing without adding a radical polymerization monomer or so-called hybrid precursor using a 3D printer. The presented approach allows printing varying mesoporous silica shapes, such as filled and hollow circles and squares, by combining DLP and LISA generating different shapes of purely mesoporous silica with large surface area. By using LISA, complicated, long post-processing after printing was avoided. Through optimization of the LISA solution composition, the needed irradiation time was reduced from 500 s down to 25 s and the mesopore order could be varied. In situ polymer functionalization was achieved by using stimuli-responsive block copolymers as functional templates. Furthermore, the mesoporous silica shape was functionalized after the printing process using silane post-grafting. By taking advantage of selective click-chemistry and shape-selective, orthogonal functionalization, analytes such as the model dye Alexa647-NHS can be identified by their shape selective binding and subsequent fluorescence imaging. The possibility of detecting analytes by shape-selective orthogonal functionalization and simply visualizing the shape of fluorescing mesoporous silica bares great potential for sensing of multiple analytes in complex solution using a combinatorial approach. The ability to produce silica shapes with designed porosity and more complex shape are expected to be useful for the development of small-scale devices for sensing and other applications. Further improvements on the fidelity of printed shapes, scalability of the process, and larger library of block copolymers for in situ functionalization of the pores are expected.

4. Experimental Section

Chemicals: All chemicals and solvents were purchased from Sigma–Aldrich, VWR, Thermo Fisher Scientific, Alfa Aesar, abcr, and Atto Tec and used as received unless stated otherwise. The solutions for the LISA process were prepared with poly(dimethoxysiloxane) (abcr), Pluronic P123 (average M_n≈5800 g mol^{-1}, Sigma–Aldrich), diphenyliodonium hexafluorophosphate (Alfa Aesar, 98%) as PAG, isopropyl-9H-thioxanthen-9-one (Sigma–Aldrich, 97%) as PS-I, technical grade of methanol and toluene (VWR, ≥98%) and distilled water. Printed mesoporous silica shapes were functionalized with (3-mercaptopropyl)trimethoxysilane (MPTS, Thermo Fisher Scientific, 95%) or (3-aminopropyl)triethoxysilane (APTES, Sigma–Aldrich, 99%) in anhydrous toluene (Sigma–Aldrich, 99.8%). This dye, Alexa Fluor 647-NHS (Thermo Fisher Scientific, 1 µg mL^{-1} in 1 M $NaHCO_3$), was used for coloring of the functionalized shapes. For

adjusting the pH value during extraction hydrochloric acid (VWR, technical, 32%) was used. For TEM sample preparation Emplura ethanol (≥99.5%, Merck) was used. Substrates for dip-coating followed by irradiation were silicon wafers (Si-Mat, Kaufering, Germany, 100 mm diameter, 525 ± 25 µm thickness, type P/Bor, <100> orientation, CZ growth method, 2–5 W resistivity, polished on one side). During the mesoporous silica printing process substrates used were microscopy slides (ground edges, 90°, 76 × 52 × 1 mm, Marienfeld, Lauda-Königshofen, Germany).

LISA Solution: The LISA solution compositions were inspired by literature[16,18] and contain following components PDMOS : Pluronic P123 : PAG : PS-I and methanol : toluene (3:1 vol/vol). The optimized LISA solution has higher PAG and PS-I molar ratios. The LISA solution for printing in situ functionalized mesoporous silica contains PEO_{42}-*b*-$PNBA_{13}$ (M_n = 4742.6 g mol^{-1}) instead of Pluronic P123 in the optimized LISA solution composition. All solution compositions are listed below. For preparing the LISA solution PDMOS, Pluronic P123 or the block copolymer and the solvent mixture were treated together in an ultrasonic bath for 10 min, before PAG and PS-I were added. This solution was kept in the dark and stirred over night at ambient temperature. Until use this solution was stored in aliquots in the freezer (−18 °C). The LISA solutions were prepared and stored in the freezer without adding water. The LISA solutions were disposed of after use.

1) LISA solution: PDMOS : Pluronic P123 : PAG : PS-I (1 : 0.0075 : 0.0015 : 0.004 molar ratio) and 30 wt% methanol : toluene (3:1 vol/vol) based on PDMOS.
2) LISA solution with 1 vol% distilled water: PDMOS : Pluronic P123 : PAG : PS-I (1 : 0.0075 : 0.0015 : 0.004 molar ratio) and 30 w% methanol : toluene (3:1 vol/vol) based on PDMOS and 1 vol% distilled water was added before use.
3) Optimized LISA solution: PDMOS : Pluronic P123 : PAG : PS-I (1 : 0.0075 : 0.0075 : 0.02 molar ratio) and 30 wt% methanol : toluene (3:1 vol/vol) based on PDMOS and 1 vol% distilled water was added before use.
4) LISA solution for in situ functionalization with PEO_{42}-*b*-$PNBA_{13}$ (M_n = 4742.6 g mol^{-1}): PDMOS : PEO_{42}-*b*-$PNBA_{13}$: PAG : PS-I (1 : 0.0075 : 0.0075 : 0.02 molar ratio) and 30 wt% methanol : toluene (3:1 vol/vol) based on PDMOS and 1 vol% distilled water was added before use.

Free-Standing Mesoporous Silica Films: The formation of mesoporous silica films was realized by LISA.[16] Both LISA solutions – with and without distilled water – were used. If distilled water was added, it was added 30 min before using the solution. Silicon wafers were washed with ethanol and dip-coated into the corresponding LISA solution using a withdrawal speed of 2 mm s^{-1} at ambient conditions. Then, the silica films were irradiated using a lamp (LUMATEC Superlite 400, Deisenhofen, Germany) with filter 1 (325–500 nm) and intensity 5 (30 mW cm^{-2}) while maintaining a distance of 10 cm between lamp and applied thin film. The lamp irradiates from the top of the applied thin film. The irradiation time and post-processing time varies for each individual solution composition as shown in Figure S1 (Supporting Information). Transparent mesoporous silica films as shown in Figure 2a were prepared by 4 min irradiation followed by 11 min resting time at ambient conditions. Samples shown in Figure 2f were prepared by 3 min irradiation followed by 5 min resting time under ambient conditions. The silica thin film still containing the mesopore template was then removed from the glass substrate by the use of a razor blade.

Printing of Mesoporous Silica: By using DLP as light source, free-standing mesoporous silica shapes were obtained. The printer was placed in a fume hood which was protected from light with a wavelength below 470 nm. The LISA solution was kept in the dark during 5 min of stirring. 1 vol% distilled water was added to the LISA solution in the specifically equipped fume hood to avoid uncontrolled irradiation during solution preparation and the solution was stirred for 5 min. To exclusively coat on one side of the substrate, blade coating was used. 0.3 mL LISA solution was spread on a glass substrate using a doctor blade (gap width 20 µm, 4 cm width, Erichsen Model 360–40 mm, Hemer, Germany). Then, the glass substrate with a thin LISA film was placed into the printer (Asiga MAX X27 equipped with a 385 nm LED, Sydney, Australia). Here, the LED irradiates from beneath the applied LISA thin film. For the best results using the LISA solution with additional 1 vol% water (Figure 3), 500 s irradiation time with an intensity of 40 mW cm^{-2} was applied. After 5 min resting time, the illuminated pattern was washed with toluene for 1 min and gently dried using pressurized air. Five minutes later the printed silica shapes, still containing mesopore template, can be removed from the glass substrate. To calcinate the template the same calcination procedure as mentioned above was used. For the optimized silica solution as used for the results shown in Figure 4, only 25 s irradiation with a light intensity of 40 mW cm^{-2} time was needed, all other parameters were used as before. Printing of the in situ functionalized silica shapes using PEO_{42}-*b*-$PNBA_{13}$ was carried out with 250 s irradiation and 40 mW cm^{-2} while the other parameters were kept the same (Figure 5).

Calcination: Calcination was used to remove the mesopores template in printed mesoporous silica shapes using LISA solutions 1–3: heating with 1 °C min^{-1} up to 100 °C, and holding this temperature constant for 1 h, heating with 1 °C min^{-1} up to 250 °C and holding this temperature constant for 4 h. Calcination of LISA solution 4, which includes the functional template PEO_{42}-*b*-$PNBA_{13}$, was carried out using this thermal treatment program: heat to 60 °C in 10 min, hold 60 °C for 1 h, heat to 130 °C in 10 min, hold 130 °C for 1 h, heat with 1 °C min^{-1} to 350 °C and hold 350 °C for 2 h.

Functionalization and Dye Linkage: To functionalize the printed and calcined mesoporous silica shapes a solution of 0.043 wt% silane (MPTS or APTES) in anhydrous toluene was used. The functionalization step was carried out under nitrogen protective atmosphere at 80 °C for 1 h. Then the mesoporous silica shapes were filtered and carefully washed with toluene. Subsequently, the silica shapes were extracted in distilled water for 15 min. To covalently bind the dye to the mesoporous silica shapes, they were placed in Alexa Fluor 647-NHS solution (1 µg mL^{-1} in 1 M $NaHCO_3$) for 1 h. Extraction of the excess, non-attached dye from the mesoporous silica was carried out in distilled water for 2 h. After extraction the mesoporous silica shapes were let dry at ambient temperature overnight.

Fluorescence Imager: Vilber Fusion FX7 Edge (Eberhardzell, Germany) was used for fluorescence detection using different filters for the chosen dye Alexa 647 (illumination c640, emission f695). Images taken with no filters under white light illumination serve only as a reference.

Attenuated Total Reflection-Infrared spectroscopy (ATR-IR): ATR-IR spectra of the (in situ functionalized) mesoporous silica shapes were recorded without any substrates using the ATR mode of a Spectrum Three Fourier transform infrared (FT-IR) spectrometer from PerkinElmer (Rodgau, Germany) in the range from 4000–650 cm^{-1} with a resolution of 0.4 cm^{-1} (10 scans). ATR-IR spectra were normalized to the asymmetric stretching vibration of Si–O–Si at 1041 cm^{-1}. Background and baseline correction were automatically performed by the software Spectrum (Version 10.5.4 by Perkin Elmer). All further data processing was performed in Origin 2023.

Transmission Electron Microscopy (TEM): TEM images were recorded using JEOL JEM 2100F transmission electron microscope (Tokyo, Japan) with a maximum resolution of 2 Å operating at an accelerating voltage of 200 kV. Samples were prepared by dispersing in ethanol. After 10 min sonification, a 3.05 mm Cu grid (mesh size 200) with a Lacey carbon film (Plano, Wetzlar, Germany) was dipped into the dispersed solution. With sample covered TEM grid was dried under ambient conditions. The pore distribution determined by TEM was evaluated by measuring at least 100 pores and plotted against their frequency.

Scanning Electron Microscopy (SEM): The SEM images were obtained using the Zeiss EVO 10 scanning electron microscope and the software SmartSEM V06.03. (Oberkochen, Germany) with a SE detector, operated at an accelerating voltage of 15–20 kV. The samples were coated with a 10–15 nm coating of Pt/Pd (from ESG Edelmetall-Service, Rheinstetten, Germany) using a Cressington 208 HR sputter coater (Cressington Scientific Instruments sold by TESCAN, Dortmund, Germany).

Small Angle X-Ray Scattering (SAXS): SAXS experiments were performed in a XEUSS 1.0 SAXS setup (XENOCS, Grenoble, France).

Monochromatic X-rays (λ = 0.15419 nm) were produced with a GENIX 3D micro-focus tube. The incoming X-ray beam was collimated to have a size at sample position of 0.5 × 0.5 mm^2. Scattered photons were detected using a PILATUS 100 K detector placed at D = 2500 mm sample to detector distance (calibrated using Silver Behenate as standard).

Argon Gas Adsorption: With argon adsorption at 87 K full isotherms in the relative pressure range from 0 to 1 were measured using an Autosorb iQ (Quantachrome sold by Anton Paar, Ostfildern-Scharnhausen, Germany). Based on the argon gas adsorption isotherms the specific surface area, pore size, and the pore size distribution were determined using BET (BET; 11 points between 0.05 and 0.3 P/P_0) and the corresponding NLDFT kernal. Before each measurement, the samples were degassed at 80 °C for 12 h under high vacuum.

Optical Microscopy: Microscopy images of printed mesoporous silica shapes were obtained by using the Olympus microscopy Bx60 (Olympus, Hamburg, Germany) (software ProgRes Capture Pro V2.8.8) in the transmitted light mode. The measurements of the obtained microscopy images were performed using ImageJ.

Supporting Information

Supporting Information is available from the Wiley Online Library or from the author.

Acknowledgements

The authors kindly acknowledge the funding from the European Research Council (ERC) under the European Union´s Horizon 2020 research and innovation program (grant agreement no. 803758). The authors thank Oleksandr Moskalyk for carrying out the synthesis of PEO_{42}-*b*-$PNBA_{13}$. Furthermore, the authors thank Claire Förster for some TGA measurements. The authors acknowledge the research group of Prof. Kleebe (Material Science, TU Darmstadt) for access to the TEM, the research group of Prof. Biesalski (TU Darmstadt) for access to their analytic lab and Prof. Azzaroni (INIFTA, La Plata Argentina) for access to the Soft Matter Laboratory facilities. J.M. acknowledges financial support for her research stay at the Instituto de Investigaciones Físicoquimicas Teóricas y Aplicadas (INIFTA-UNLP/CONICET) in La Plata, Argentina by German Research Foundation (DFG) within the Collaborative Research Centre 1194 "Interaction between Transport and Wetting Processes", Project-ID 265191195. M. C. is a staff member of CONICET Argentina. For the help during SEM measurements, the authors would like to thank Felix Krusch. The authors would also like to thank Matthias Kremer for helpful discussions.

Open access funding enabled and organized by Projekt DEAL.

Conflict of Interest

The authors declare no conflict of interest.

Data Availability Statement

The data that support the findings of this study are available from the corresponding author upon reasonable request.

Keywords

digital light processing, in situ functionalization, light-induced self-assembly, mesoporous silica, printing, sol-gel chemistry

Received: November 30, 2023
Revised: January 26, 2024
Published online: February 13, 2024

[1] a) J. P. Kennedy, L. Williams, T. M. Bridges, R. N. Daniels, D. Weaver, C. W. Lindsley, *J. Comb. Chem.* **2008**, *10*, 345. b) R. Liu, X. Li, K. S. Lam, *Curr. Opin. Chem. Biol.* **2017**, *38*, 117.
[2] R. Potyrailo, K. Rajan, K. Stoewe, I. Takeuchi, B. Chisholm, H. Lam, *ACS Comb. Sci.* **2011**, *13*, 579.
[3] C.-H. Su, C.-L. Sun, Y.-C. Liao, *ACS Omega* **2017**, *2*, 4245.
[4] a) M. Benz, A. Asperger, M. Hamester, A. Welle, S. Heissler, P. A. Levkin, *Nat. Commun.* **2020**, *11*, 5391; b) A. S. Abd-El-Aziz, M. Antonietti, C. Barner-Kowollik, W. H. Binder, A. Böker, C. Boyer, M. R. Buchmeiser, S. Z. D. Cheng, F. D'Agosto, G. Floudas, H. Frey, G. Galli, J. Genzer, L. Hartmann, R. Hoogenboom, T. Ishizone, D. L. Kaplan, M. Leclerc, A. Lendlein, B. Liu, T. E. Long, S. Ludwigs, J.-F. Lutz, K. Matyjaszewski, M. A. R. Meier, K. Müllen, M. Müllner, B. Rieger, T. P. Russell, D. A. Savin, et al., *Macromol. Chem. Phys.* **2020**, *221*, 2000216.
[5] W. Lei, A. Deckers, C. Luchena, A. Popova, M. Reischl, N. Jung, S. Bräse, T. Schwartz, I. K. Krimmelbein, L. F. Tietze, P. A. Levkin, *Adv. biol.* **2022**, *6*, 2200166.
[6] W. F. Maier, K. Stöwe, S. Sieg, *Angew. Chem. Int. Ed.* **2007**, *46*, 6016.
[7] B. Sartori, H. Amenitsch, B. Marmiroli, *Micromachines* **2021**, *12*, 740.
[8] L. Zu, W. Zhang, L. Qu, L. Liu, W. Li, A. Yu, D. Zhao, *Adv. Energy Mater.* **2020**, *10*, 2002152.
[9] B. P. Bastakoti, Y. Li, N. Miyamoto, N. M. Sanchez-Ballester, H. Abe, J. Ye, P. Srinivasu, Y. Yamauchi, *Chem. Commun.* **2014**, *50*, 9101.
[10] P. Xu, H. Yu, X. Li, *Anal. Chem.* **2011**, *83*, 3448.
[11] a) C. J. Brinker, Y. Lu, A. Sellinger, H. Fan, *Adv. Mater.* **1999**, *11*, 579; b) L. Nicole, C. Boissière, D. Grosso, A. Quach, C. Sanchez, *J. Mater. Chem.* **2005**, *15*, 3598.
[12] D. Grosso, F. Cagnol, G. J. d. A. A. Soler-Illia, E. L. Crepaldi, H. Amenitsch, A. Brunet-Bruneau, A. Bourgeois, C. Sanchez, *Adv. Funct. Mater.* **2004**, *14*, 309.
[13] H. de Paz-Simon, A. Chemtob, C. Croutxé-Barghorn, S. Rigolet, L. Michelin, L. Vidal, B. Lebeau, *APL Mater.* **2014**, *2*, 113306.
[14] a) H. de Paz, A. Chemtob, C. Croutxé-Barghorn, S. Rigolet, B. Lebeau, *Microporous Mesoporous Mater.* **2012**, *151*, 88; b) H. de Paz-Simon, A. Chemtob, F. Crest, C. Croutxé-Barghorn, L. Michelin, L. Vidal, S. Rigolet, B. Lebeau, *RSC Adv.* **2012**, *2*, 11944.
[15] H. de Paz-Simon, A. Chemtob, C. Croutxé-Barghorn, S. Rigolet, L. Michelin, L. Vidal, B. Lebeau, *J. Phys. Chem. C* **2014**, *118*, 4959.
[16] M. Sibeaud, H. de Paz-Simon, C. Croutxé-Barghorn, S. Rigolet, L. Michelin, B. Lebeau, L. Vidal, P.-A. Albouy, A. Chemtob, *Microporous Mesoporous Mater.* **2018**, *257*, 42.
[17] M. Sibeaud, C. Croutxé-Barghorn, S. Rigolet, L. Michelin, B. Lebeau, L. Vidal, A. Chemtob, *Microporous Mesoporous Mater.* **2018**, *267*, 235.
[18] S. Shi, X. Allonas, C. Croutxé-Barghorn, A. Chemtob, *New J. Chem.* **2015**, *39*, 5686.
[19] F. Kotz, K. Arnold, W. Bauer, D. Schild, N. Keller, K. Sachsenheimer, T. M. Nargang, C. Richter, D. Helmer, B. E. Rapp, *Nature* **2017**, *544*, 337.
[20] I. Cooperstein, E. Shukrun, O. Press, A. Kamyshny, S. Magdassi, *ACS Appl. Mater. Interfaces* **2018**, *10*, 18879.
[21] E. Shukrun, I. Cooperstein, S. Magdassi, *Adv. Sci.* **2018**, *5*, 1800061.
[22] D. G. Moore, L. Barbera, K. Masania, A. R. Studart, *Nat. Mater.* **2020**, *19*, 212.
[23] E. S. Farrell, N. Ganonyan, I. Cooperstein, M. Y. Moshkovitz, Y. Amouyal, D. Avnir, S. Magdassi, *Appl. Mater. Today* **2021**, *24*, 101083.
[24] E. Shukrun Farrell, Y. Schilt, M. Y. Moshkovitz, Y. Levi-Kalisman, U. Raviv, S. Magdassi, *Nano Lett.* **2020**, *20*, 6598.
[25] L. Zhao, J. J. Mikolei, M. Ceolin, R. Pardehkhorram, L. Czerwenka, A. Andrieu-Brunsen, *Microporous Mesoporous Mater.* **2024**, *366*, 112923.
[26] M. Thommes, K. Kaneko, A. V. Neimark, J. P. Olivier, F. Rodriguez-Reinoso, J. Rouquerol, K. S. Sing, *Pure Appl. Chem.* **2015**, *87*, 1051.

